Flexural Capacity and Ductility of HPS-70W Bridge Girders

AARON J. YAKEL, PATRICK MANS and ATOROD AZIZINAMINI

ABSTRACT

The development of High Performance Steel (HPS), which boasts high yield strengths (70 and 100 ksi), while maintaining ductility and toughness combined with an available weathering finish offers many potential opportunities to steel bridge design. Many of these benefits have yet to be realized due to the limitations in design specifications placed on the use of steels with yield strength above 50 ksi. This paper reports on the experimental results and associated finite element analysis of four girders intended to address the limitations placed on girders in negative bending, e.g., girders spanning over a pier in multiple span bridges. All of the girders tested were able to attain their predicted strength as determined using the AASHTO *LRFD Bridge Design Specifications* (AASHTO, 1998). However, the compact section tested did not exhibit the amount of ductility implied by the equations. Based on the results of the tests and analyses performed, the limitations with regards to strength could be removed while the compact provisions allowing moment redistribution may require additional investigation.

INTRODUCTION

In 1994, a cooperative research program between the Federal Highway Administration (FHWA), the U.S. Navy, and the American Iron and Steel Institute (AISI) was initiated. One of the products of this cooperative work was the development, in 1996, of a new grade of steel. This steel is referred to as High Performance Steel (HPS) and is identified commercially as HPS-70W steel. The availability of this new and enhanced grade of steel has created both opportunities and challenges for the steel industry.

For years, 70-ksi steel has been available on the market. However, the construction community had been reluctant to utilize it in bridge construction. One of the main reasons for this reluctance is the weldability characteristics of conventional 70-ksi steel. High performance steel contains less carbon than other high strength steels previously used in bridge construction. The lower carbon content greatly improves the weldability of HPS. The other enhanced characteristic of HPS is its high toughness, which provides very high resistance to brittle fracture, allowing structures to tolerate a high level of damage without the risk of sudden failure. Finally, HPS-70W is a weathering steel suitable for use in the unpainted condition.

On the structural design side, the *LRFD Bridge Design Specification*, issued by the American Association of Highway and Transportation Officials, henceforth referred to as the AASHTO Specification, provides provisions that must be followed in the design and construction of steel bridges (AASHTO, 1998). Some of the provisions for the design of steel bridges given in the AASHTO Specification are empirical. In other words, the provisions were developed based on experimental results from tests conducted primarily on steels with yield strength levels of less than or equal to 50 ksi. Because of the lack of test data, sections of the AASHTO Specification currently contain limitations, which restrict the use of high yield strength steels in bridge construction, thus limiting the full utilization of the advantages HPS offers in steel bridge construction. In 1996, a research study was initiated at the University of Nebraska-Lincoln to address these limitations.

As part of this research, four girders have been tested to determine their ultimate load carrying capacity and ability to undergo inelastic deformation.

In addition to the direct results obtained from physical testing, another purpose of testing the four specimens presented in this report was to develop experimental data that could be used to verify numerical models. These numerical models are being used to comprehend the influence of yield strength, element slenderness, and other parameters of the high performance steel on the flexural behavior of steel plate girders.

SPECIMEN SELECTION

The four girders can be broken into two pairs. The selection process was slightly different for each pair.

The first pair of specimens were both fabricated using 70 ksi steel. Both specimens had compact flanges with one

Aaron J. Yakel is research engineer and PhD candidate, University of Nebraska-Lincoln, department of civil engineering, Lincoln, NE.

Patrick Mans is engineer, KCI Technologies, Inc., Mechanicsburg, PA. Formerly graduate student, University of Nebraska-Lincoln, department of civil engineering, Lincoln, NE

Atorod Azizinamini is professor, University of Nebraska-Lincoln, department of civil engineering, Lincoln, NE.

having a compact web and the other a noncompact web. The final size of the specimens was then determined by the availability of the High Performance Steel at the time of fabrication.

The goal in testing the second pair of girders was to compare the behavior of a girder fabricated from 70 ksi material with the behavior of a 50 ksi girder. To accomplish this, a 50/70 ksi pair was designed such that they would be as similar as possible. Both girders in the second pair had noncompact webs and compression flanges.

Factors Affecting Selection of the Test Specimens

This section discusses the factors that were considered in the selection and design of the test specimens.

- Web Slenderness – Depth over thickness
- Flange Slenderness – Outstanding width over thickness
- Length over Depth
- Distance between Lateral Bracing
- Aspect ratio – Depth over width of compression flange
- Compression flange thickness over web thickness
- a_r – Twice the area of web in compression over area of compression flange in elastic range
- a_{rp} – Same as a_r except calculated using a fully plastic section

The significance of these parameters is discussed in the following sections.

In the selection of the 50/70 ksi specimen pair, the above parameters were made as similar as possible. The AASHTO Specification defines flange slenderness as one half the total flange width divided by its thickness. Web slenderness is defined as two times the depth of the web in compression divided by the web thickness. For noncompact sections, the depth of web in compression comes from a linear elastic distribution. For compact sections, the depth of web in compression is that calculated at the theoretical plastic moment.

Figure 1 shows the section classification limits based on web and flange slenderness ratios. The AASHTO Specification does not provide provisions for the design of girders having a web or compression flange which fall outside of the noncompact boundary. The slenderness limits for a compact section are given by Equations 1 and 2 for the flange and web respectively.

$$\frac{b_f}{2\ t_f} \leq 0.382\sqrt{\frac{E}{F_{yc}}} \tag{1}$$

$$\frac{2D_{cp}}{t_w} \leq 3.76\sqrt{\frac{E}{F_{yc}}} \tag{2}$$

where

b_f = Width of Compression Flange

t_f = Flange Thickness

E = Modulus of Elasticity

F_{yc} = Specified Minimum Yield strength of the Compression Flange

D_{cp} = Depth of web in compression at the theoretical plastic moment

t_w = web thickness

Similarly, the slenderness limits for a noncompact section are given by Equations 3 and 4 for the flange and web respectively.

$$\frac{b_f}{2t_f} \leq 1.38\sqrt{\frac{E}{F_{yc}\sqrt{\frac{2D_c}{t_w}}}} \tag{3}$$

$$\frac{2D_c}{t_w} \leq 6.77\sqrt{\frac{E}{F_{yc}}} \tag{4}$$

where

D_c = Depth of web in compression based on linear elastic assumption

The criterion used in setting the compact limits shown in Figure 1 is the plastic rotational capacity of steel sections. Compact sections are assumed to have, at least, an inelastic rotational ductility of three (Yura, Galambos, and Ravindra, 1978). Inelastic rotational ductility is a measure of how much deformation can be experienced before the moment capacity drops below the plastic moment. Figure 2 illustrates the definition of inelastic rotational ductility.

Lateral Bracing

The lateral bracing was placed at the limit for inelastic analysis given by Equation 5. While this equation was originally developed to assure an inelastic rotational capacity of

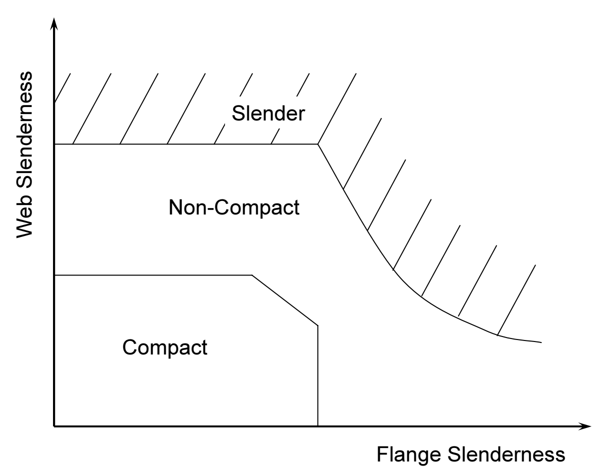

Fig. 1. Section Classification Limits.

3.0, the equation is also required for the use of the alternative strength formula, or "Q" formula in the AASHTO Specification.

$$L_b \le \left[0.124 - 0.0759\left(\frac{M_l}{M_P}\right)\right]\left(\frac{r_y E}{F_{yc}}\right) \tag{5}$$

where

L_b = lateral unbraced length
M_l = lower moment due to the factored loading at either end of the unbraced length
M_P = plastic moment
r_y = minimum radius of gyration of the steel section with respect to the vertical axis
E = modulus of elasticity
F_{yc} = specified minimum yield strength of the compression flange

Length Over Depth (*L/D*)

The specimens tested for this report were intended to simulate the interior pier region (between inflection points) of a two-span girder. It is assumed that this pier region extends a distance $0.2L$ to either side of the pier where L is the length of each span. Using this assumption, the girders tested would have an equivalent L/D ratio of 37.5. This span to depth ratio (37.5) is larger than the typical practical value (20 to 30). However, the larger span length resulted in a lower shear eliminating the concern over shear interaction, which can limit the section capacity when the applied shear and moment are both near their ultimate values.

Cross-Sectional Ratios

The remaining parameters can be considered collectively as cross-sectional ratios, as they deal with the relationships between different aspects of the cross section.

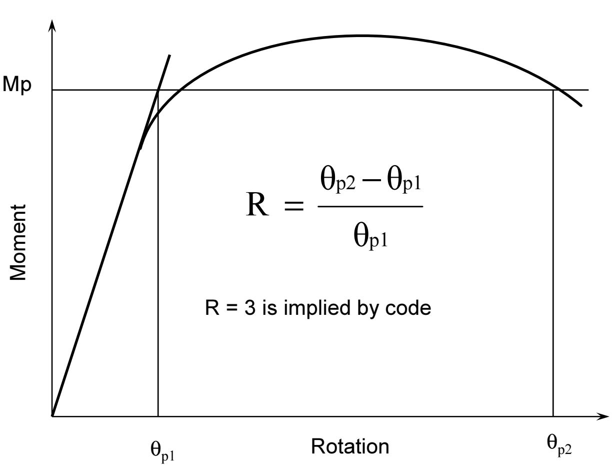

Fig. 2. Inelastic Rotational Ductility.

The ratio D/b_f is the aspect ratio of the section where D is the total web depth and b_f is the compression flange width. While rolled wide flange shapes often have aspect ratios as low as 1.0, forming a square profile; common bridge girders are more likely to be tall rectangles with aspect ratios between 2.0 and 4.0. The aspect ratio gives some sense of the strong axis versus weak axis stiffness.

The parameters a_r and a_{rp} have similar definitions. The parameter a_r is twice the area in compression over the area of the compression flange while the girder remains elastic. The parameter a_{rp} is two times the area of web in compression at the theoretical plastic moment over the area of the compression flange. For symmetric sections, these two values are identical. The final parameter, t_{fc}/t_w, is the compression flange thickness (t_{fc}) over the web thickness (t_w). In a physical sense, the previous three parameters (a_r, a_{rp}, and t_{fc}/t_w) can give an indication of the level of restraint that exists between the elements, which make up the cross section.

SELECTED TEST SPECIMEN GEOMETRY

Specimens A and D were to be the first in a series of specimens which investigated the behavior of both compact and noncompact sections fabricated using HPS-70W steel, with a large effort being placed on verifying the compactness requirements. After testing of compact Specimen D resulted in a plastic rotational capacity quite less than that required of a compact section, the focus of the study turned to the behavior of noncompact sections. To this end, a pair of specimens were designed which had a web slenderness midway between compact and noncompact along with a flange slenderness ratio located near the noncompact limit. The parameters were chosen to result in an efficient section typical of actual bridge girders.

Table 1 summarizes the physical dimensions of the test specimens. A typical specimen is shown in Figure 3, which depicts the dimensions and bracing of Specimen C50. Due to limitations on the availability of 70-ksi steel, the end regions of Specimen C70, where material was expected to remain elastic, utilized 50-ksi steel. All other specimens were fully homogeneous.

The target web slenderness for Specimens C50 and C70 was 1.25 times the compact web limitation. This corresponds to a nominal slenderness of 113.2 and 95.6 for 50 ksi and 70 ksi materials respectively. The web of Specimen D was made compact with a slenderness of 76.6 while the web of Specimen A was chosen to be 90.7, or 1.2 times the compact limit.

The target flange slenderness for Specimens C50 and C70 was 95 percent of the noncompact limit. These values correspond to a nominal flange slenderness of 9.8 and 8.5 for 50 ksi and 70 ksi materials respectively. The compres-

Table 1. Test Specimen Dimensions and Resulting Parameters

		Flange		Web		Length			Yield Strength		Slenderness: Actual Specimens		Slenderness: Compact Limit		Slenderness: Non-Compact Limit		Slenderness: Compact Ratio		Cross Sectional Parameters			
		Width	Thickness	Depth	Thickness	Span	L_{b1}	d_o	Flange	Web	Flange	Web	Flange	Web	Flange	Web	Flange/NC Limit	Web/ Compact	L/D	D/b_f	A_r	t_f/t_w
		[in]	[in]	[in]	[in]	[in]	[in]	[in]	[ksi]	[ksi]	--[a]	--[a]	--[a]	--[a]	--[a]	--[a]	--[a]	--[a]	--[a]	--[a]	--[a]	--[a]
A	Design	16.250	1.500	34.000	0.375	744	126	126	70	70	5.42	90.7	7.78	76.5	9.10	137.8	0.60	1.18	21.9	2.09	0.52	4.00
	Actual	16.250	1.530	34.000	0.390	744	126	126	71.3	82.3	5.31	87.2	7.70	75.8	9.11	136.5	0.58	1.15	21.9	2.09	0.53	3.92
D	Design	16.250	1.500	28.750	0.375	636	144	144	70	70	5.42	76.7	7.78	76.5	9.49	137.8	0.57	1.00	22.1	1.77	0.44	4.00
	Actual	16.250	1.540	28.750	0.393	636	144	144	71.3	82.3	5.28	73.2	7.70	75.8	9.51	136.5	0.55	0.96	22.1	1.77	0.45	3.92
C50	Design	14.750	0.750	35.375	0.3125	530	168	48	50	50	9.83	113.2	9.20	90.6	10.19	163.0	0.97	1.25	15.0	2.40	1.00	2.40
	Actual	14.844	0.77	35.250	0.330	530	168	48	49.9	64.7	9.68	106.8	9.21	90.6	10.35	163.2	0.94	1.18	15.0	2.37	1.02	2.32
C70	Design	12.750	0.750	29.875	0.3125	448	102	48	70	70	8.50	95.6	7.78	76.5	8.98	137.8	0.95	1.25	15.0	2.34	0.98	2.40
	Actual	12.688	0.76	29.813	0.331	448	102	48	81.9	84.7	8.30	90.1	7.19	70.8	8.43	127.4	0.99	1.27	15.0	2.35	1.02	2.31

[a]Non-Dimensional

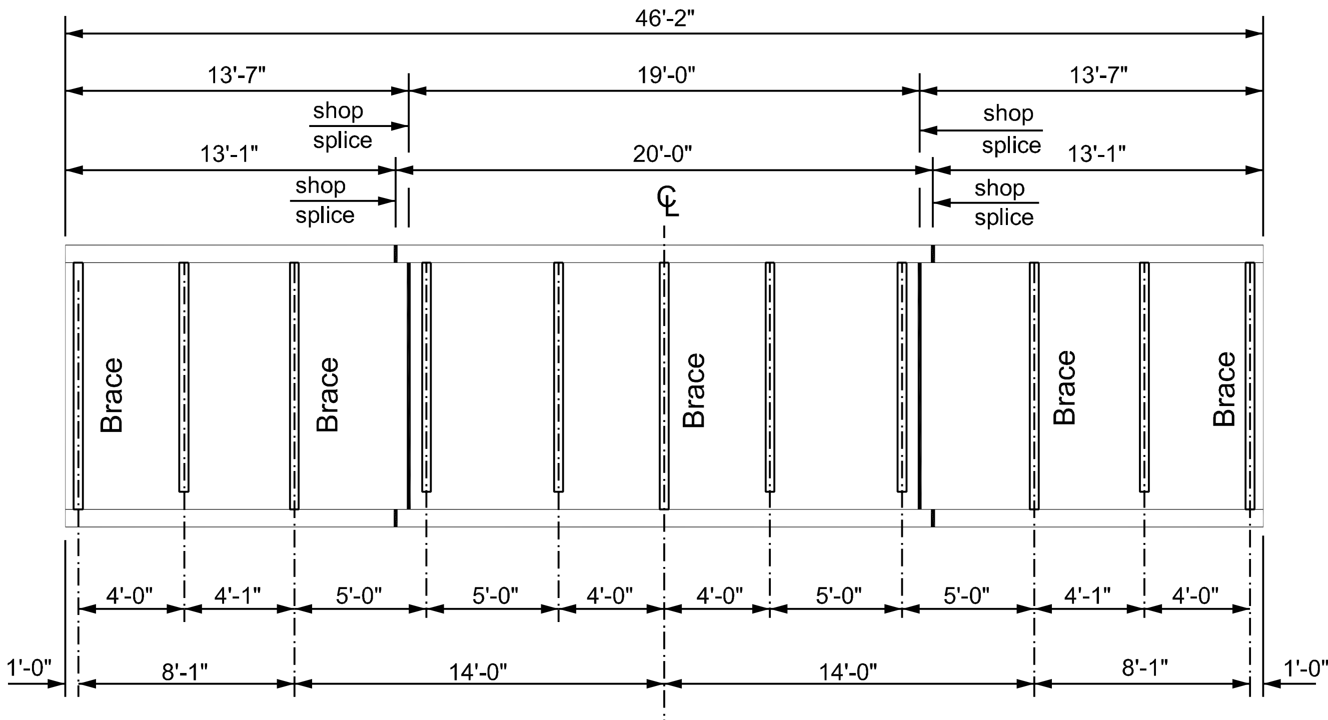

Fig. 3. Specimen C50.

sion flange of Specimens A and D were both designed to be 75 percent of the compact limit, or 5.4.

Table 1 gives the resulting slenderness values when the actual dimensions and material properties are taken into account. In each case, it can be seen that use of actual properties resulted in specimens that were more slender than designed. For comparison among the specimens, Table 1 also lists some additional parameters of the specimens.

SPECIMEN FABRICATION

Test girders A, D, and C70 were fabricated by Lincoln Steel Company. Egger Steel Company fabricated girder C50. Since the plate sizes used are not uncommon in bridge girder fabrication, typical fabrication methods were utilized.

Butt welds were full-penetration submerged arc welds. A preheat of 200°F was used, which was within the 125°F to 400°F range as required by the Bridge Welding Code (AWS, 1995). Web-to-flange welds were submerged arc fillet welds with approximately 110°F preheat. Undermatched filler material was used on the 70-ksi specimens. Low hydrogen flux was used on the full-penetration welds as recommended in the report, Weld Parameter Investigation for HPS-70W Steel (Nickerson, 1997).

Stiffener welds were ¼-in. SMAW. The stiffeners were connected to the tension flange at lateral brace locations to aid in the transfer of the lateral bracing loads.

EXPERIMENTAL TESTING

Test Setup

Each specimen was tested as a simply supported beam with a single point load applied at midspan. The system allowed end rotations and longitudinal displacement and provided intermediate lateral supports. Instrumentation included strain gages on the flanges and web. These are concentrated near the centerline to capture the primary area of interest. Potentiometers were used to determine the rotation at the ends and the deflection at the quarter points. The applied loads were obtained from pressure cells placed in the hydraulic system. The reactions at the ends of the beam were monitored using load cells. A detailed description of each of the components is contained in the following sections.

Bracing System

A bracing system consisting of a roller assemblage moving along a guiding system was designed as part of the test setup. The guiding system was attached to the strong floor of the laboratory, and the roller assemblage was bolted to the stiffeners on the girders. The roller assemblage allowed the girders to move freely up and down as well as parallel to their longitudinal axis. Figure 4 is a photograph of the first lateral brace away from the load. This bracing point went through several revisions due to the high lateral loads, which were experienced at extreme deflections during testing.

Loading System

Initially the loading configuration for Specimen A consisted of two hydraulic rams pushing down on the specimen. At a relatively high load and inelastic displacement level, concern for safety resulted in unloading the specimen and modifying the loading arrangement. To create a more stable test setup, a new loading configuration was assembled consisting of four hydraulic rams placed in the basement. The rams reacted against the strong floor pulling downwards on a stiff spreader beam located on the top flange of the girder. Although the location of the rams was changed, the point of load application to the specimen remained the same. This loading configuration is the same for the final three specimens and can be seen in Figure 5.

The midspan deflections were anticipated to be large and the stroke on the rams was limited to 12 inches. For this rea-

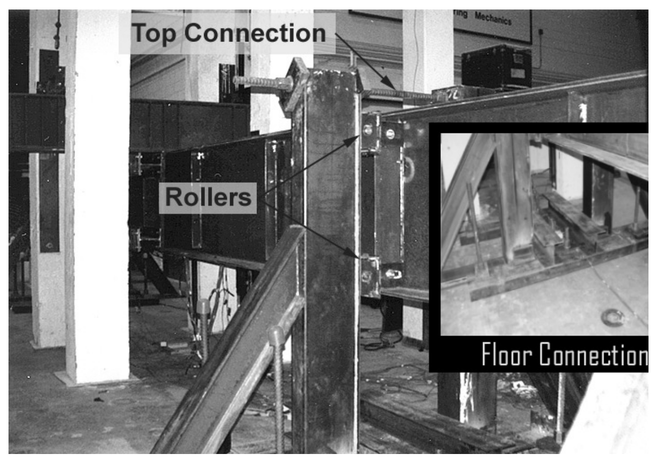

Fig. 4. Lateral Bracing

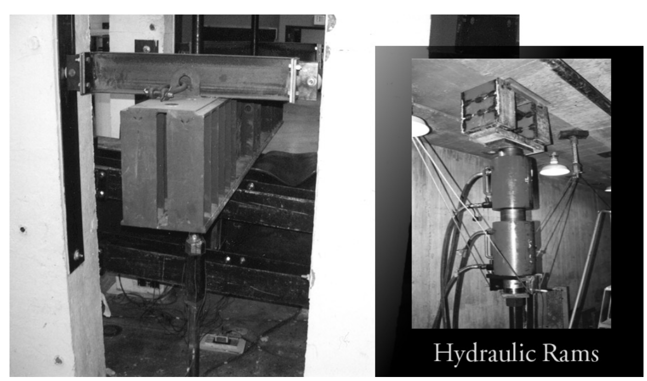

Fig. 5. Loading Point Rams (inset).

son, prestressing chairs were used to prevent unloading of the specimen during the restroking of the rams. The inset of Figure 5 shows the rams and the prestressing chairs used during the modified test setup for girder A.

Instrumentation

In order to determine the rotation that the girder underwent during testing, potentiometers were placed at both ends of the specimen. Figure 6 shows the typical layout at each end. The differential deflection between a pair of potentiometers and the distance between them was used to calculate the beam end rotation.

The vertical deflections at the quarter points were also measured using potentiometers. By connecting the potentiometer located at midspan to a plotter, a continuous load displacement plot was recorded. Strain gages were placed at various locations on the web and flanges. Figure 7 shows the strain gage layout for Specimen C50. This layout is typical of the other specimens as well. Pressure and load cells were used to monitor the applied loads. Pressure cells were placed on the hydraulic lines to each ram going to the pressure side. One pressure cell was placed on the manifold of the return line to monitor backside pressure. Load cells were placed under the rams on each of the load rods. As a final check, strain gages were placed on the loading rods themselves. The data from all instrumentation were collected using a data acquisition system and stored in a computer for later analysis.

Testing Procedure

Each specimen was tested as a simply supported beam with a concentrated load applied at midspan. The load was applied using hydraulic rams and monitored by pressure and load cells. Loads were applied at approximately 15 kip increments during the elastic regions. Following the yielding of the specimens, the loading was based on incrementing the midspan deflection. The use of prestressing chairs, as shown in Figure 5, allowed re-stroking the hydraulic rams without having to unload the specimen. Loading of each specimen continued until a significant drop in load-carrying capacity of the specimens was observed.

TEST RESULTS

Reported test results include plots of load versus displacement, moment versus rotation and load versus resulting strains. The rotation reported is the summation of the rotation from each end.

Figure 8 shows the load deflection curves for each of the specimens. The following paragraphs describe the key observations made during the testing.

Specimen A

Additional instrumentation was used to monitor the out-of-plane movements of the web on this girder. This instrumentation detected the initiation of local web buckling at a load of 406 kips, which corresponded to a vertical midspan deflection of about 9.3 in. This was after the load deflection curve had begun to display non-linearity. Local buckling of the compression flange was observed shortly after local web buckling was initiated. The load associated with the initial buckling of the compression flange was 410 kips.

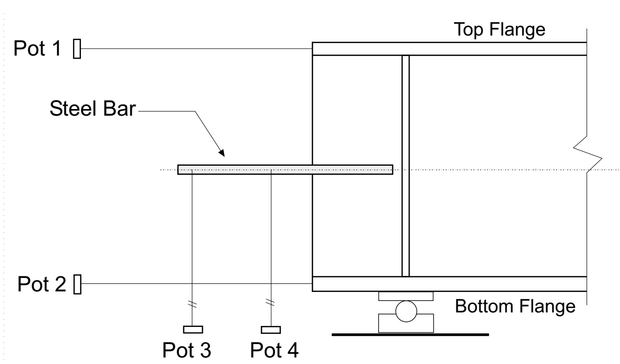

Fig. 6. Rotation Measurement at Ends.

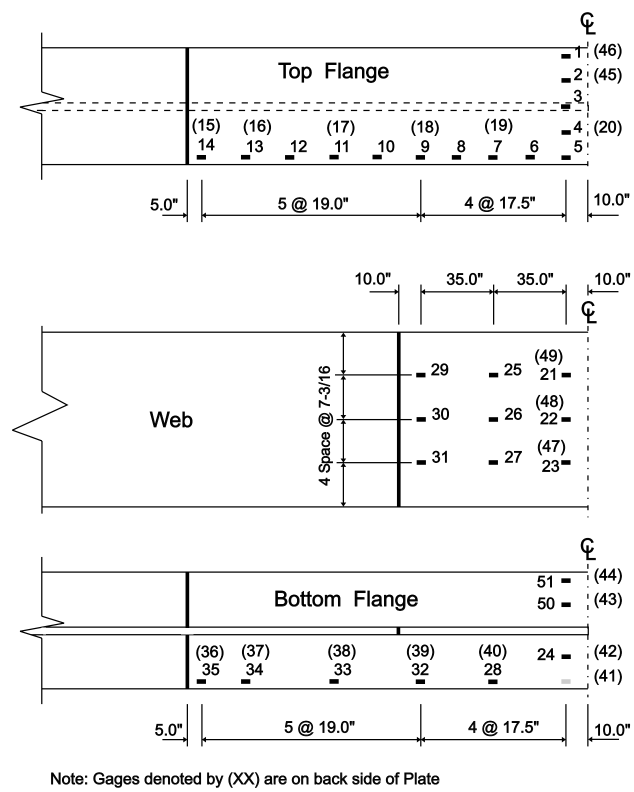

Fig. 7. Strain Gage Placement, Specimen C50.

This caused a vertical midspan deflection of about 12 in. In order to re-stroke the hydraulic rams, the specimen was unloaded at a vertical midspan deflection of approximately 15 in. Upon reloading, the specimen reached the same load level before exhibiting additional non-linearity. The decrease in load-carrying capacity between midspan deflections of 15 and 17 in. is believed to be the result of lateral movement of the bracing points at either side of midspan. At this load, very high levels of lateral forces were present at the bracing points. These high lateral forces pushed the columns supporting the lateral braces in the direction perpendicular to the longitudinal axis of the girder.

As noted previously, the first setup for test Specimen A consisted of loading the girder from the top. At a midspan displacement of approximately 17 in., due to safety concerns, the specimen was unloaded. The lateral bracing points, showing signs of movement, were stiffened and the loading arrangement was changed. The modified loading system was then used on subsequent specimens and was the system described earlier. It can be seen that after the stiffening of the lateral bracing system and reloading, the specimen exhibited a higher load-carrying capacity. Loading of the specimen continued until a midspan displacement of 21.5 in. was achieved at a load of 270 kips. At this time it was decided to conclude the testing and unload the girder. The maximum applied load was 417 kips, which occurred at a deflection of approximately 14.4 in.

Specimen D

Local compression flange and web buckling occurred after the girder exhibited nonlinear load deflection behavior. Local buckling of the compression flange and local web buckling were observed almost simultaneously. Lateral-torsional buckling did not initiate until the loading was well beyond the initial yield, at around 17 in. The test was terminated at a deflection of approximately 24 in. under a load of about 285 kips. The maximum applied load was 433.5 kips, which occurred with a deflection of approximately 13.5 in.

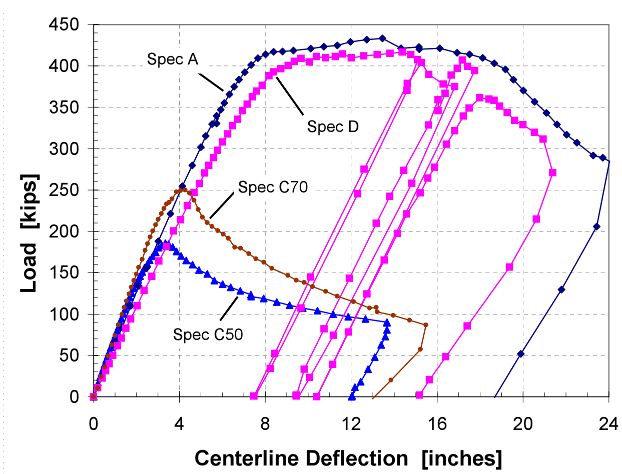

Fig. 8. Load Deflection Plots.

Specimen C70

At a midspan deflection of approximately 2 in., which corresponds to a load of about 148 kips; it was observed that mill scale was coming off the flanges. This is evidence of large strains and often is the first sign of yielding. At a load of 249 kips, and a midspan deflection of 4 in., initial compression flange buckling was observed. This occurred after yielding had already set in as evidenced by nonlinearity in the load deflection curve. Shortly after this, at a load of 246 kips and a vertical midspan deflection of about 4.5 in., lateral-torsional buckling was observed.

Before the maximum extension on the rams was reached, the test was halted to restroke the rams. This occurred twice during the test, at loads of 167 and 108 kips, with midspan deflections of 7.6 and 13.0 in. respectively. The midspan deflection at the end of the test was approximately 15.5 in. and the load had dropped to about 87 kips. The maximum applied load was 250 kips, which caused a vertical midspan deflection of approximately 4.3 in.

Specimen C50

During the test of this specimen, local compression flange and web buckling occurred almost simultaneously with the attainment of the maximum load. This occurred shortly after the load deflection curve exhibited nonlinearity. Loading was continued and the rams were restroked at a midspan deflection of 7.3 inches. The maximum midpoint deflection, prior to unloading, was 13.7 in. and occurred at a load of about 89.5 kips. The maximum applied load was 185.6 kips, which had caused a midspan deflection of approximately 3.3 in.

DISCUSSION OF RESULTS

Specimens A and D

Test Specimen A had compact flanges and a noncompact web. According to AASHTO Specifications, this specimen was required to develop, at a minimum, the yield moment capacity of the cross section. Further, for noncompact sections, AASHTO Specifications do not require any inelastic rotational capacity. Since Specimen D was compact, one would expect this girder to reach its plastic moment capacity and have a greater available rotation capacity than Specimen A.

Figures 9 and 10 show the extent of local web and flange buckling in the vicinity of the loading points following the test conclusion. Figure 11 shows the profile of the compression flange for each specimen measured after the test conclusion.

Figure 12 shows the moment rotation response of Specimens A and D. The moment is nondimensionalized with respect to the plastic moment capacity of the girder. The plastic moment capacity of the girder was calculated based on the actual material properties and measured specimen dimensions. Results of material tests conducted to obtain the stress strain characteristics of the steel used in the fabrication of the test girders are shown in Figure 13. The calculated plastic moment capacities of the specimens are 69,424 in.-kips and 58,098 in.-kips for Specimens A and D respectively. Also shown in Figure 12, the inelastic rotational ductility of Specimen A, as defined in Figure 2, is about 1.2 and the ductility of Specimen D was 1.9.

It should again be noted that the lateral bracing points immediately adjacent to midspan were spaced based on the inelastic lateral bracing requirements as given by Equation 5. This spacing requirement is also a requirement for use of the Alternative "*Q*" Formula. Although the inelastic provision results in a smaller spacing than that required

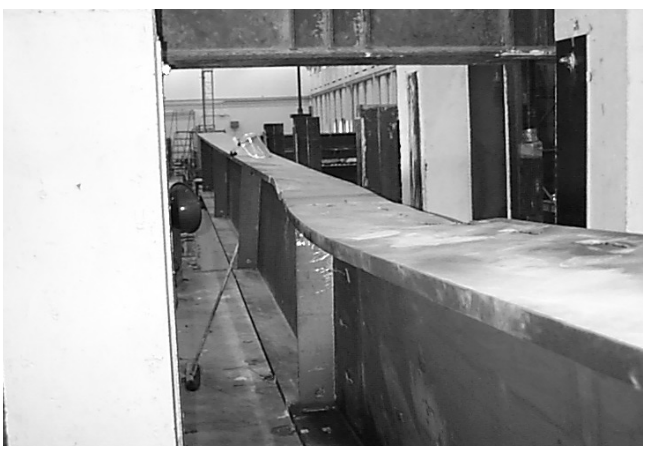

Fig. 9. Specimen A after Testing.

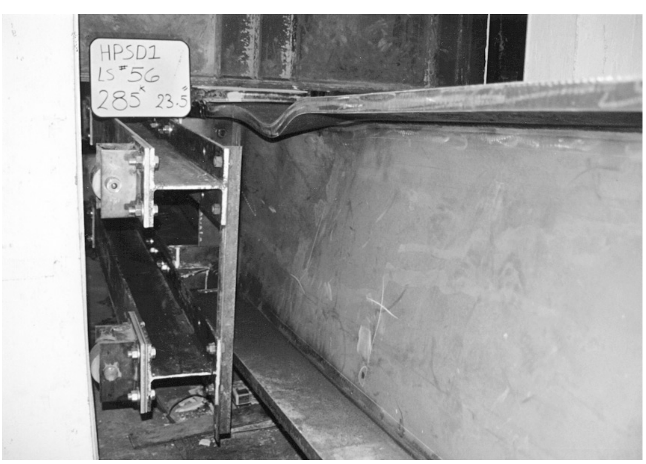

Fig. 10. Specimen D after Testing.

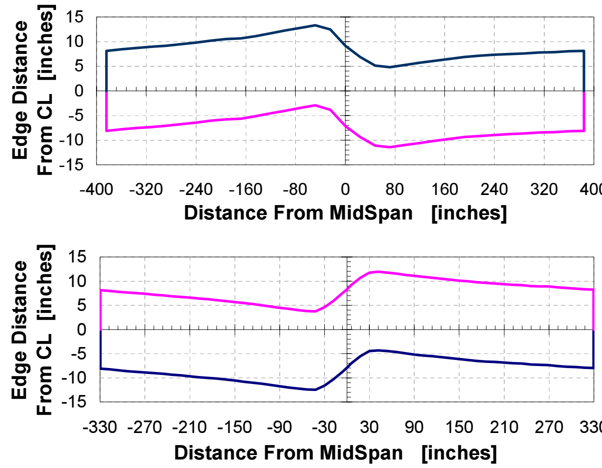

Fig. 11. Compression Flange Profiles of Specimens A (Top)and D (Bottom).

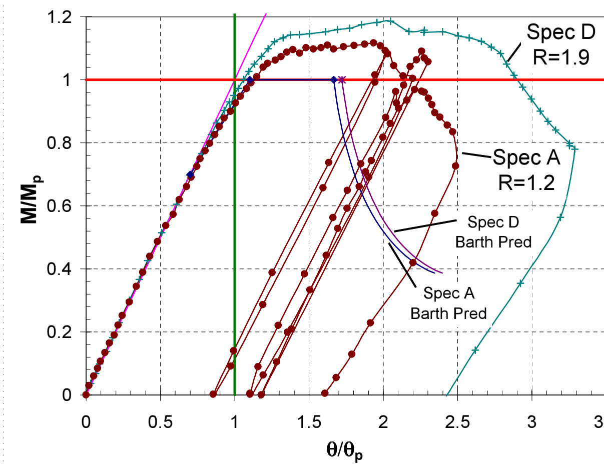

Fig. 12. Moment Rotation (Specimens A and D).

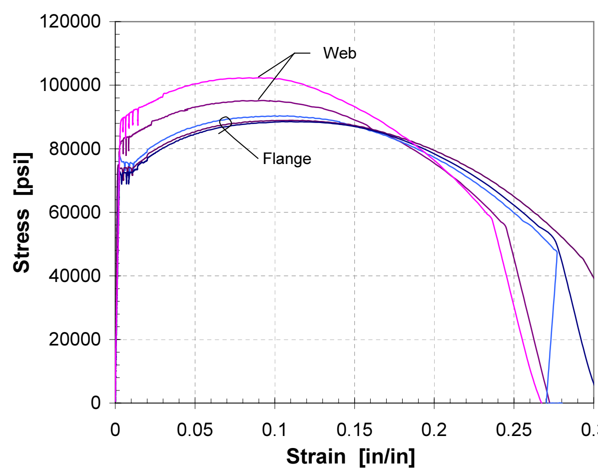

Fig. 13. Material Properties (Speciments A and D).

for noncompact sections, comparison of the test results with the "Q" formula was desired. The maximum spacing of lateral bracing for Specimen A, based on the noncompact section requirements of the AASHTO Specification, is 13.5 ft. The inelastic bracing requirement, results in a maximum unbraced length of 10.5 ft.

Specimens C50 and C70

Test Specimens C50 and C70 were noncompact. According to AASHTO Specifications, these specimens were expected to develop only the yield moment capacity of the section. Furthermore, for noncompact sections, AASHTO Specifications do not require any inelastic rotational capacity. Indeed, both C50 and C70 were capable of reaching their corresponding yield moment.

Figures 14 and 15 show the extent of local web and flange buckling in the vicinity of the loading point following the conclusion of the test of Specimen C50. From these figures, it can be seen that the failure was asymmetric with all large local element deformations occurring on one side of midspan.

Figure 16 shows the profile of the compression flange, measured after the test conclusion. To one side of midspan very little deformation occurred, while on the other side, there was a sudden lateral shift. The results from C70 look virtually the same and are not shown.

Figure 17 shows the moment rotation response of the C50 and C70 specimens. The moment is normalized with respect to the plastic moment capacity of the girder. The plastic moment capacity of the girder was calculated based on the actual material properties. Material test results conducted to obtain the stress strain characteristics of the steel used in fabrication of the test girders are shown in Figure 18. The material samples were obtained from steels used to fabricate the flanges of the girder in the test regions.

Fig. 14. Photo of Specimen C50 at Midspan After Test.

Fig. 15. Photo of Specimen C50 at Midspan After Test (side).

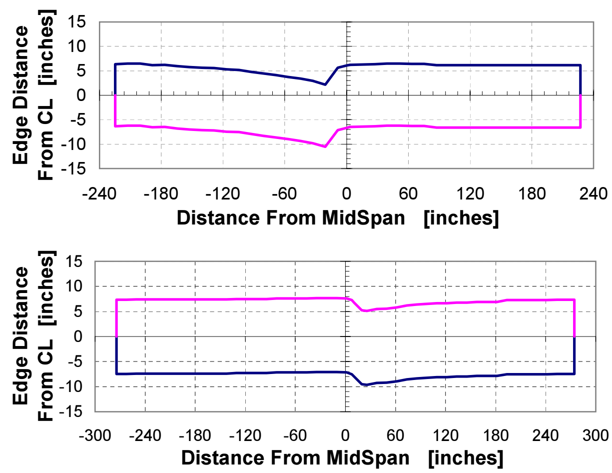

Fig. 16. Lateral Profile of Compression Flange Specimen C50 (top) and C70 (Bottom)

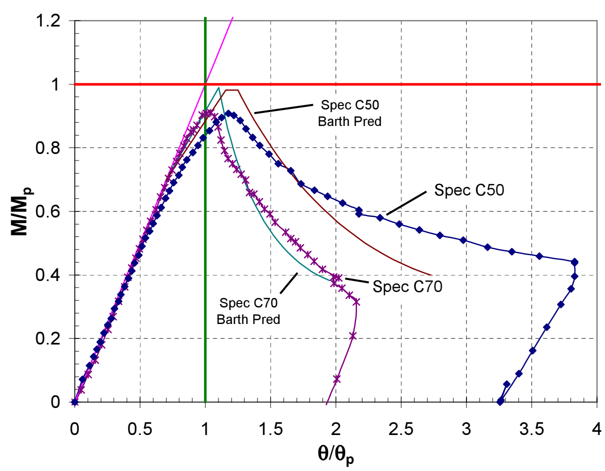

Fig. 17. Moment Rotation (Specimens C50 and C70).

Table 2. Comparison of Predicted Strength

			M_{Max}	M_P	M_Y	AASHTO	*Q* Formula	AISC App F	AISC App G	Barth Prediction
A	Value	[Kip-in]	77530	69424	63965	63965	69424	67346	63965	69424
	Ratio	[---]	1.00	1.12	1.21	1.21	1.12	1.15	1.21	1.12
D	Value	[Kip-in]	68920	58098	53465	53465	58098	57994	53465	58098
	Ratio	[---]	1.00	1.19	1.29	1.29	1.19	1.19	1.29	1.19
C50	Value	[Kip-in]	24600	27090	23310	23310	25560	25610	22320	26590
	Ratio	[---]	1.00	0.91	1.06	1.06	0.96	0.96	1.10	0.93
C70	Value	[Kip-in]	27970	30730	27730	27730	27570	28950	25920	30460
	Ratio	[---]	1.00	0.91	1.01	1.01	1.01	0.97	1.08	0.92

Note: Ratio = M_{max}/M_{pred}

The calculated plastic moment capacities of the girders based on actual material properties are 30,728 in.-kips and 27,095 in.-kips for Specimens C70 and C50, respectively.

Comparison of Predicted Moment Capacity

Five methods were used to predict the moment capacity of the test specimens. Table 2 shows the results of these comparisons. Descriptions of the methods used to predict the moment capacity are as follows.

The first method calculates the strength using the provisions of the AASHTO Specification. Specimens A, C50, and C70 were all noncompact which therefore restricted the predicted capacity to their respective yield moments. Compact Specimen D should have been able to reach its theoretical plastic moment and provide an inelastic rotation value of at least three.

The second method is the AASHTO Alternative Formula for Flexural Resistance as specified in the AASHTO Specification. This formula predicted that both Specimens A and D should be able to reach the plastic moment capacity.

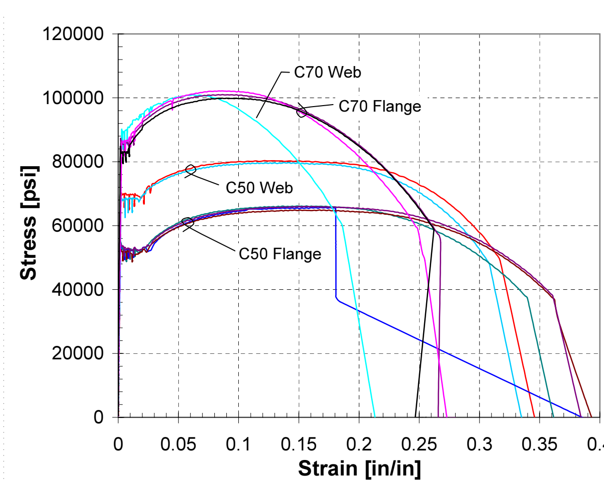

Fig. 18. Material Test Results.

The third method is the AISC Load and Resistance Factor Design Provisions as specified in Appendix F (AISC, 1993). For Specimens A and D the flange slenderness and lateral bracing were under the compactness limit and therefore did not affect the capacity. The web of Specimen A was noncompact resulting in a predicted capacity 96 percent of the plastic moment. The web of Specimen D, however, was compact thereby resulting in a predicted capacity equal to the theoretical plastic moment. Both the web and flange of Specimens C50 and C70 were noncompact. The controlling element for Specimen C50 was the web, while the flange controlled the strength of the C70 specimen.

The fourth method is the AISC Load and Resistance Factor Design Provisions as specified in Appendix G (AISC, 1993). While this method is specified for sections with slender webs, the development of the method is quite similar to the others and it was included for comparison.

The final approach used to predict the flexural capacity of the test specimens was based on moment rotation curves suggested by Barth (1996). This method also predicts the plastic rotation capacity. Figures 12 and 17 show the results of this prediction for each of the specimens. As seen in the figures, Barth's equation gives a good prediction of the response of Specimens C50 and C70. On the other hand, Barth's approach underestimates the rotational capacity of Specimens A and D. Note that the prediction for Specimen C70 does not have a plateau region.

Table 2 indicates that the AASHTO Specification for predicting flexural capacity of compact and noncompact sections could be extended to high performance steels, as the ratio of flexural capacities obtained from testing over predicted values ranges between 1.01 and 1.29.

Figure 17 shows the normalized moment versus the normalized plastic rotation for Specimens C50 and C70. By comparing the results for these specimens, it can be seen that the two girders behaved very similarly. In particular, the maximum normalized moment was almost identical at 91 percent of the theoretical plastic moment.

NUMERICAL ANALYSIS

The main objective in carrying out these analyses is to develop a tool that could assist in investigating the effects of different parameters influencing the flexural behavior of plate girders. A reliable numerical model should be able to predict both global behavior (such as load deflection) and local behavior (such as local strains and stresses) consistent with results obtained experimentally.

In the following sections, steps taken in developing the finite element model are described, together with a comparison of the test and numerical results. Since the development of the modeling techniques is ongoing, the description of these techniques represents what is current at the time of writing.

Development of the Numerical Model

The finite element analysis program ANSYS Version 5.6 was used to conduct these numerical analyses. Shell elements were used to model the entire plate girder including the stiffeners. Results of this investigation indicated that using offset beam elements as stiffeners could significantly alter the results. Further, use of shell elements for stiffeners allowed for an accurate accounting of the stiffening effect that intermediate stiffeners provide for flanges and any web-flange interaction that may result.

The element type selected is ANSYS's 4-node SHELL181 with 6 degrees of freedom per node (ANSYS, 1999). This element is capable of accounting for large strains and finite rotations. Full integration with incompatible modes was utilized for all elements. This element displayed good convergence through the entire analysis. Figure 19 shows a typical model.

Stress-Strain Curve

The element formulation used in the numerical analyses requires knowledge of the true-stress and true-strain characteristics of the material. This was obtained from the engineering stress strain data empirically by performing a finite element analysis simulating the actual uniaxial material tests. This procedure is described more fully in *Flexural Capacity of HPS-70W Bridge Girders* (Yakel, Mans, and Azizinamini, 1999). A typical resulting true stress strain-curve used in the finite element analysis is shown in Figure 20.

The flange and web material models have been implemented as multilinear isotropic hardening models. The stiffener material is represented as a bilinear material model. The Von Mises yield criterion and J2 flow rule complete the plasticity model.

Geometric Imperfections

The following method was used to model the geometric imperfections. An eigenvalue buckling analysis was performed on the girder for a downward load applied at midspan. The resulting first eigenvector was then scaled down such that the maximum displacement was one eighth of an inch. These displacements were superimposed on the original geometry thus creating a distorted specimen. In addition to the buckled shape, additional distortions, shown in Figure 21, were introduced. The imperfection variation was sinusoidal between points of restraint and alternated in orientation. For example, the web bulge alternated sides at each stiffener location with zero deformation at the stiffener. The maximum magnitude within each section was randomly selected within the limits given in Table 3. This resulted in an unsymmetrical imperfect test specimen. It has

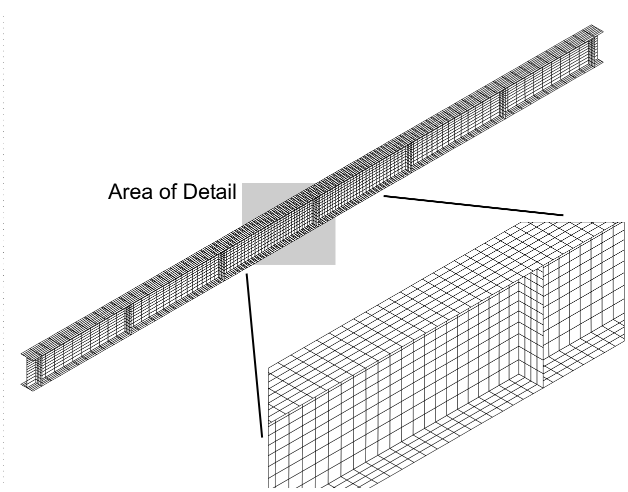

Fig. 19. Typical Finite Element Model.

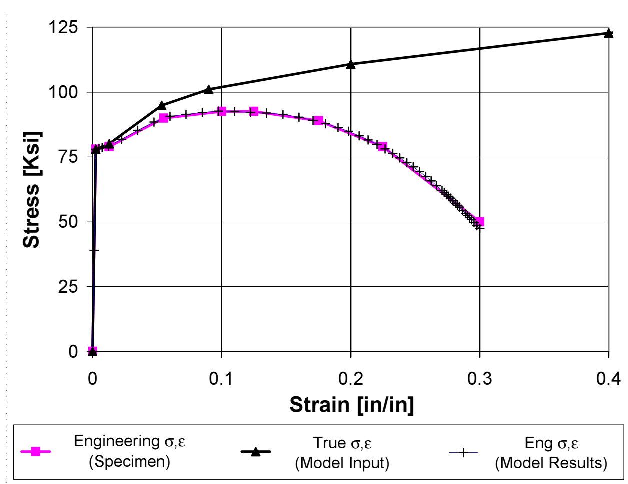

Fig. 20. FEM True-Stress True-Strain.

Table 3. Magnitude of Geometric Imperfections

Mode of Imperfection	Maximum Amplitude Between Inflection Points [inches]	Inflection Points
Web Bulge	$\frac{Min\left(D,d_0\right)}{150}$	Web Stiffeners
Flange Tilt	$\frac{L_b}{1000}$	Lateral Bracing Locations
Flange Sweep	$Min\left(\frac{b_{fc}}{150},\frac{Lb}{500}\right)$	Lateral Bracing Locations
Lowest Buckling Mode	$\frac{1}{8}$	—

been found that the use of perfect symmetry in numerical modeling can have an impact both on failure mode and load-carrying capacity. Several runs were made on each specimen with different random values of imperfection applied. For each run on a particular specimen the failure mode and capacity were similar.

Residual Stresses

The effect of residual stress manifests itself in the moment rotation and load deflection diagrams as a "rounding off" of the curve as the girder yields. This effect can result in a lower capacity, especially in moderately noncompact sections. The applied residual stresses used in the model are shown in Figure 22. This pattern is similar to that presented by Barth (1996). It has been found, by applying varying amounts of residual stress, that the magnitude of residual stress has no effect on the ultimate moment capacity of the girders under investigation.

Effect of Non-Ideal Lateral Bracing

During the experimental testing of Girder A at large deformations, the level of lateral loads created at bracing points was much larger than anticipated. The expected value was 2 percent of the load in the compression flange. Given a yield stress of 70 ksi, no more than 45 kips were expected. However, the analysis shows the possibility of generating a lateral force in excess of 100 kips. During the experimental test, the lateral loads were high enough to actually move the

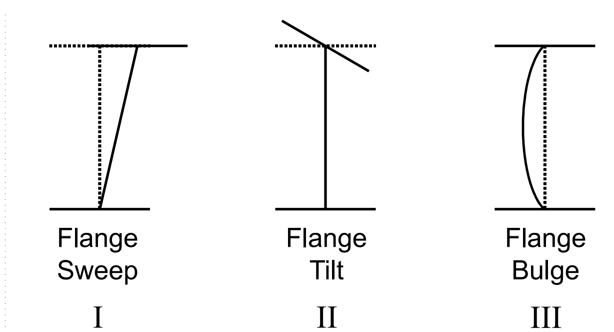

Fig. 21. Geometric Imperfections.

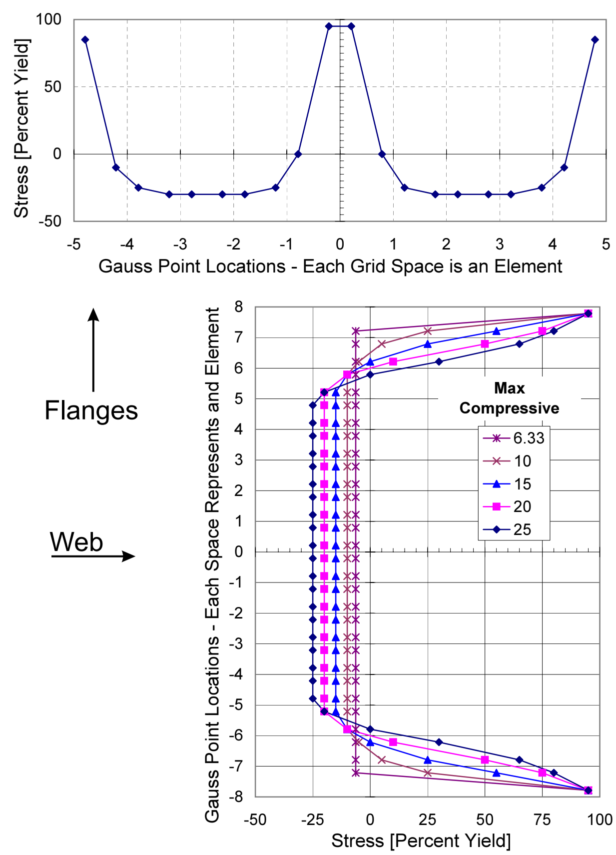

Fig. 22. Residual Stresses.

lateral restraints in test A and reduce their effectiveness. A number of analyses were run to study the effect of non-ideal lateral bracing. It was determined that had the lateral braces remained fixed during the test, little difference would have been noted in the ultimate load while the ductility could have been increased from 1.2 to 1.4, which is still well below the required 3.0 (Yakel, Mans, and Azizinamini, 1999). Figure 23 shows a plot of lateral forces developed at the bracing points versus the girder deflection, which was obtained from analysis assuming fixed bracing. It can be seen that the lateral loads are very small until large deformation levels are reached. At this point, the lateral forces begin to increase quite dramatically.

Discussion of Finite Element Analysis Results

In this section of the report, results are presented of the numerical analysis carried out for the four test girders. The previous section described the procedures used to select the model for these analyses while this section provides a discussion of the results and comparison with experimental test data.

Load Deflection Comparison

As seen in Figure 24, a very good correlation is observed between the initial stiffness obtained from experimental testing and numerical analyses for all specimens. The finite element results yield earlier and then parallels the experimental results at a lower load. Although the load level of the analysis is below that of the experimental testing, the general behavior of the curves are similar and begin to unload at approximately the same strain as that obtained during the experiment.

Deformed Shape

The finite element models used in this investigation produced a good prediction of both local and global behavior. Figure 25 shows a comparison of the deformed shape of Specimen C70 as observed from experimental tests and those obtained from finite element analysis. The results represent the same level of midspan displacement. The results from Specimen C70 were representative of the same comparison performed on the remaining specimens. As mentioned earlier the finite element analysis aspect of this project is still in progress. However, the modeling technique used in this investigation was adequate to give a good prediction of the experimental results at both the local and global levels.

The numerical analyses are being used to investigate the effect of additional parameters on the flexural and rotational capacity of steel plate girders.

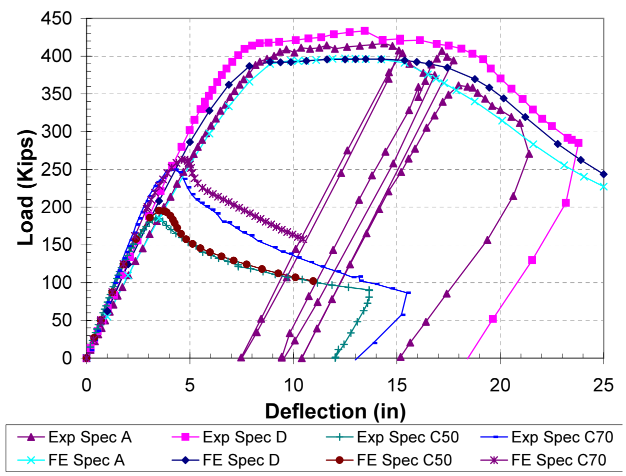

Fig. 24. Finite Element Load Deflection Results.

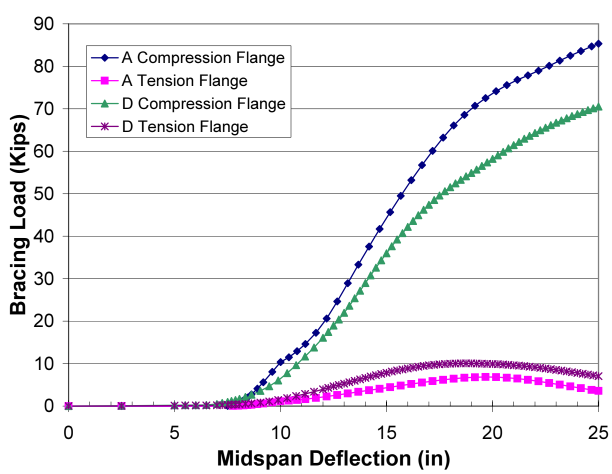

Fig. 23. Lateral Force at Bracing Point.

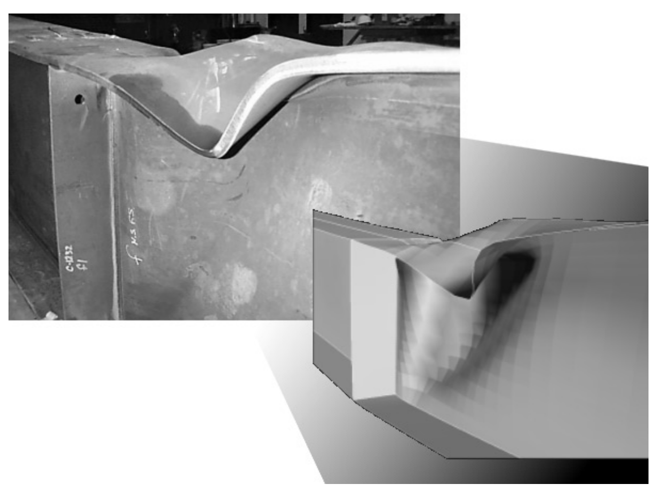

Fig. 25. Deformed Shape Comparison (Specimen C70)

CONCLUSIONS

This report provides a summary of the four steel plate girders tested at the University of Nebraska-Lincoln and associated numerical studies. These tests were part of an investigation to evaluate the limitations in AASHTO LRFD Bridge Design Specifications related to use of steels with yield strength exceeding 50 ksi.

Two pairs of specimens were tested. The first pair, Girders A and D were both fabricated of 70-ksi material. Specimen D was compact in both the flange and web. Specimen A had a compact flange and a noncompact web. The key details being investigated with this set of specimens were their inelastic rotation and ultimate moment capacities.

Both specimens were able to reach and exceed their theoretical plastic moment capacity, although the current provisions do not require this of the noncompact Specimen A. Neither specimen, however, was able to provide an inelastic rotational ductility of three, which is implied by the AASHTO Specification for compact sections. This ductility requirement would have to have been fulfilled by Specimen D to allow moment redistribution.

For the second pair of specimens, C70 was fabricated from 70-ksi high performance steel and C50 was fabricated using 50-ksi steel. The specimens were designed such that they were as similar as possible. The most important similarity parameters were the normalized web and flange slenderness ratios. The symmetric specimens were tested in three point bending with the load applied at midspan. Lateral bracing was provided which met the inelastic bracing requirement for compact design, or use of the Q formula.

Comparing the behavior of the two girders, one finds many similarities. Both Specimens C50 and C70 were capable of exceeding their yield moment capacity as would be required by the AASHTO Specifications for noncompact sections. In fact, the maximum load normalized against the theoretical plastic moment was the same for both girders. Further, the failure mode and unloading behavior were similar for both of the specimens.

Based on the results presented in the paper, and those reported by Yakel, Mans, and Azizinamini (1999 and 2000), the following recommendations were made to the AASHTO T-14 Committee and are reflected in the AASHTO LRFD Bridge Design Specification (2000 Interim).

Noncompact 50-ksi and 70-ksi plate girders exhibit similar behaviors. Therefore, equations deemed acceptable for the design of 50-ksi girders should be applicable to 70-ksi girders.

Noncompact 70-ksi plate girder sections can provide the yield moment capacity as calculated using the AASHTO LRFD Specification.

Compact 70-ksi plate girder sections can provide the plastic moment capacity as calculated using the AASHTO Specifications.

Compact 70-ksi plate girders are unable to provide inelastic rotational ductility of three, as implied by the AASHTO Specification for compact sections. Therefore, the 10 percent moment redistribution stated in Section 6.10.4.4 of the AASHTO Specifications should not be allowed for plate girders fabricated using 70-ksi steels.

ACKNOWLEDGMENTS

Funding for this investigation was provided primarily by the U.S. Department of Transportation, the Federal Highway Administration (FHWA), the American Iron and Steel Institute (AISI), the National Steel Bridge Alliance (NSBA), Lincoln Steel, the Mid-America Transportation Center (MATC), the Nation Bridge Research Organization (NaBRO), and the Center for Infrastructure Research (CIR). The authors would like to express their appreciation for this support. The authors would also like to express their thanks to Mr. Milo Cress, of the local FHWA office, Mr. Mustafa Jamshidi and Mr. Lyman Freeman of the Bridge Division at the Nebraska Department of Roads (NDOR), and Mr. Bud Thompson of Lincoln Steel for their assistance.

REFERENCES

AASHTO (1998), *LRFD Bridge Design Specifications*, AASHTO, 2nd Ed., Washington D.C.

AISC (1993), *Load and Resistance Factor Design Specification for Structural Steel Buildings*, Chicago, IL.

AWS (1995), *Bridge Welding Code*, D1.5.

ANSYS Inc. (1999), ANSYS Structural Analysis Guide, Canonsburg, PA.

Barth, K. E. (1996), *Moment-Rotation Characteristics for Inelastic Design of Steel Bridge Beams and Girders*, Ph.D. dissertation, Purdue Univ., West Lafayette, IN, 311.

Nickerson, R. L. (1997), *Girder Fabrication Report #2*, Lincoln Steel Company.

Yakel, A. J., Mans, P., and Azizinamini, A. (1999), *Flexural Capacity of HPS-70W Bridge Girders*, National Bridge Research Organization, Lincoln, NE.

Yakel, A. J., Mans, P., and Azizinamini, A. (2000), *Comparison of Flexural Capacity of HPS-70W and A709-50W Bridge Girders*, National Bridge Research Organization, Lincoln, NE.

Yura, J. A., Galambos, T. V., and Ravindra, M. K. (1978), "The Bending Resistance of Steel Beams," *Journal of the Structural Division*, ASCE, Vol. 104, ST9, September, pp. 1355-1370.